Weld-end solidification cracking in pulsed-tandem gas-metal-arc welding of naval steels

Zoran Sterjovski [a,*], Christopher Bayley [b], Joe Donato [a], Nathan Lane [c, d] and Darren Lang [e]

[a] *Maritime Division, DSTO, Department of Defence, 506 Lorimer Street, Fishermans Bend, Victoria, 3207 Australia*
[b] *DRDC –Atlantic, Dockyard Laboratory Pacific, PO Box 17000 Stn Forces, Victoria, BC, Canada V9A 7N2*
[c] *Facullty of Engineering, University of Wollongong, Northfields Avenue, NSW 2500 Australia*
[d] *DMTC Ltd, Level 2, 24 Wakefield St, Hawthorn VIC 3122 Australia*
[e] *Forgacs Engineering Pty Ltd, Old Punt Road, Tomago, NSW 2322 Australia*

ABSTRACT

Pulsed tandem gas metal arc welding (PT-GMAW) has the potential to increase productivity and minimize distortion in the fabrication of naval surface ship panels. In this study, the PT-GMAW process was used in pulse-pulse mode to butt-weld 5 mm DH36, 8 mm HSLA65, 9.5 mm 350WT and 11 mm HSLA65 steel plate with ER70S-6 wire in order to assess its suitability as a replacement for submerged arc welding (SAW) and gas metal arc welding (GMAW) in panel lines of Australian naval shipyards. In the pulse-pulse mode, the wire feed rates for the leading and trailing welding wires are set independently and they alternately transfer metal into a single molten weld pool at deposition rates almost comparable with single-wire SAW. Radiographic inspection and subsequent analyses of the 8 mm, 9.5 mm and 11 mm single-bead butt-welds unexpectedly showed varying degrees of weld-end solidification cracking, which occurred within ~30 mm from the run-off tab and was different to weld-crater cracking. The percentage of plates with solidification cracking was greater at larger plate thicknesses due mainly to increases in both the weld bead depth:width ratio and joint restraint as plate thickness is increased. Also, relatively low levels of nickel in the weld metal resulted in less severe solidification cracks compared with weld metal with higher levels of nickel. There was no evidence of solidification cracks in the 5 mm welded plates. Potential strategies to overcome weld metal solidification cracking near the run-off tab in the PT-GMAW of steel are presented.

Keywords

Pulsed tandem gas metal arc welding

Solidification cracking

Naval hull steels

HSLA65 steel

DH36 steel

Single-bead welds

* *Corresponding author. Tel.: +61 3 9626 7502; fax: +61 3 96268341; E-mail: zoran.sterjovski@dsto.defence.gov.au*

1. Introduction

The pulsed tandem gas metal arc welding (PT-GMAW) process, which is commercially available but not yet optimized for wide-spread implementation into naval surface ship construction, has the potential to replace conventional arc welding processes such as submerged arc welding (SAW) and gas metal arc welding (GMAW). The appeal of the PT-GMAW process stems from its affordability compared with other high speed processes such as laser-hybrid GMAW, and an ability to (i) achieve lower levels of weldment distortion, (ii) deliver high deposition rates (comparable to SAW), and (iii) perform out-of-position welding. In the PT-GMAW process, the wires (electrodes) are fed from separate wire feed units through to two contact tubes, which are electrically isolated inside a single torch head. The power sources for both wires (electrodes) are synchronized, thus enabling the coordinated transfer of metal from each wire into a single weld pool. The system is most stable when the metal transfer between the wires is completely out-of-phase, although shielding gas type will also influence arc stability [1]. Previous studies by Sterjovski et al. [2,3] have reported both relatively low levels of welding-related distortion (compared with multi-run GMAW) and deposition rates of ~15 kg/hour with a 400 A PT-GMAW system.

Lower levels of welding-related distortion should significantly reduce delays to schedule since the dependence on line-heating/flame straightening to rectify distortion is alleviated. Moreover, it is reported by Sampath [4] that line-heating can be detrimental to the structural integrity of the hull if incorrectly applied. Less distortion in hull sections will improve the stealth characteristics of naval surface ships by reducing their radar cross-section [5]. It is also envisaged that naval surface ships with significantly less hull distortion will reduce hydrodynamic drag, and consequently improve speed and fuel efficiency than ships with greater levels of hull distortion.

Naval shipbuilders can benefit from the high deposition rates of the PT-GMAW process by producing single-pass welds of low cross-section or by increasing welding travel speeds. The latter approach, which would result in the deposition of multiple beads during the welding of plates $\geq$8 mm in thickness, is more likely to ensure adequate impact toughness in the weld metals of conventional shipping steels (e.g. DH36 and CSA 350WT) [6]. However, single-bead PT-GMAW of higher-strength steels (e.g. HSLA65) should result in weldments with adequate impact toughness since the composition of the ER70S-6 weld metal (WM) is bolstered via mixing (i.e. increased dilution) with the more highly alloyed parent steel [7].

A preliminary study by Larkin et al. [8] which assessed the feasibility of the PT-GMAW process as a replacement for SAW for single-bead butt-welding of 5 mm DH36 steel showed that high weld quality and good mechanical properties can be achieved. This achievement, combined with a significant reduction in weld-related distortion compared with corresponding SAW weldments, has resulted in the PT-GMAW process replacing SAW on some panel lines in the fabrication of naval surface ships in Australia.

The aim of the current work is to assess the suitability of the PT-GMAW process in different areas of naval surface ship construction, in particular the PT-GMAW of steel plate 8–11 mm in thickness. The successful implementation of PT-GMAW in other areas of the naval shipyard is dependent on overcoming 'teething' problems such as susceptibility to weld overlap, and WM solidification cracking at the weld-ends during the single-bead butt-welding of hull plate ($\geq$8 mm thick). The sole focus of this paper is to discuss the extent and nature of weld metal solidification cracking that occurred during the PT-GMAW of naval hull steels. Weld metal solidification cracking can be defined as cracking that occurs during the solidification of the molten weld bead. Solidification cracking is due to critical levels of strain accumulation in the solidifying weld pool as a result of thermal contraction within the material as well as externally applied loads [9]. Solidification cracks initiate above the solidus temperature of the WM or due to the presence of low melting temperature intergranular eutectic films created by the segregation of impurity (e.g. S and P) and alloying elements (C, Ni and Nb) [10]. Accordingly, WM solidification cracking is considered a complex cracking phenomenon dependent on parent steel and WM composition, solidification structures, segregation, dendrite size and orientation, joint restraint, weld travel speed, arc energy heat input and weld thickness [11,12].

2. Experimental Methods

2.1. Materials and welding

The current investigation into the optimization of the PT-GMAW process for naval shipbuilding encompasses both currently-used and future naval shipbuilding steels. The currently-used grades of steels included in this study are DH36 steel [13] and CSA 350WT steel [14]. HSLA65 steel [15] is the potential hull steel considered for this study. The reasons for the selection of HSLA65 as a potential steel for naval surface ships in Australia have previously been published [7]. The plate thicknesses and

chemical compositions of the steels used for this study are listed in Table 1. Even though the chemical composition of the two HSLA65 steels is different, they both comply with ASTM A945/A945M-06 [15].

For all welding experiments, a single torch head attached to two Fronius Trans Synergic 4000 power supply and wire feed systems was used. The two welders were synchronized to coordinate the metal transfer from each electrode to the molten weld pool (Fig. 1). For synchronized metal transfer, a synergic control system is implemented to ensure that a stable welding condition is maintained irrespective of the wire feed rates or average current levels. Coordinated metal transfer is particularly important for arc stability due to the proximity of the leading and trailing arcs (~5-6 mm). The welding parameters for each unit can be individually adjusted because each wire has its own electrically insulated contact tip within the single torch head. A high-speed-welding tractor was used to reach the required travel speeds.

ER70S-6 wire (1.2 mm in diameter) and a shielding gas containing 16% CO_2, 2.75% O_2 and 81.25% Ar were used for all single-bead full penetration butt-welds. The ER70S-6 wire was selected as it is currently being used to weld fabricate DH36, and it also meets the strength and toughness requirements for HSLA65 steel and CSA 350WT. The nominal chemical composition of the ER70S-6 wire is shown in Table 2.

In total, 20 butt-welds at least 350 mm in length were evaluated for the current work (listed in Table 3). All butt-welds were single-bead and full-penetration (square-butt preparation with a varying root gap depending on plate thickness). The single-bead approach has been used in the current study as it will lead to the biggest gains in productivity. It is also envisaged that this process will eventually compete with other processes capable of low-distortion and high-productivity single-bead welding, such as laser hybrid GMAW as its affordability improves. Table 4 lists all the critical weld process parameters for each of the welds (5 mm DH36, 8 mm HSLA65, 9.5 mm CSA 350WT and 11 mm HSLA65). All plates were clamped during welding, had tacked run-off and run-on tabs, and had machined weld preparations.

2.2. Radiography, optical emission spectroscopy, microscopy and fractography

All butt-welds were subjected to visual inspection and radiography in order to assess their quality. The radiographic technique used was XR2/S (x-ray with Type 2 film/single wall) in accordance with

AS2177-2006 [16]. All of the 9.5 mm welds and four of the 8 mm welds were tested in Canada, but met the requirements of AS2177-2006 [16].

The majority of the welds were then sectioned, metallographically prepared, etched in 2% Nital and evaluated by optical microscopy. Scanning electron microscopy (SEM) was also used to study the fracture surfaces in each of the cracked welds. Chemical compositions of each of the weld metals were determined by optical emission spectroscopy. Energy dispersive spectroscopy (EDS) was carried out on the fracture surfaces of the solidification cracks.

3. Experimental Results

3.1. Weld macrographs

Macrographs of the 5, 8, 9.5 and 11 mm welds shown in Fig. 2(a-d) reveal that each of the welds are single-bead full penetration butt-welds, and that they are free of any significant defects. In the macrographs in Fig. 2 it is evident that weld bead depth-to-width ratio increases as plate thickness increases. The weld bead depth:width ratio measured for the 5 mm, 8 mm, 9.5 mm, and 11 mm welds is 3.3, 3.3, 4.4 and 6.8, respectively.

3.2. Weld metal compositions

The chemical composition analysis of the WM region in the 5 mm, 8 mm, 9.5 mm and 11 mm welds is shown in Table 5.

3.3. Weld metal microstructure

The WM microstructures of all the full-penetration butt-welds in the current work are shown in the photomicrographs in Fig. 3. These photomicrographs are taken from the weld centerline and the center of the weld with respect to weld length. From these photomicrographs it is evident that each of the weld beads is comprised of combinations of acicular ferrite, grain boundary ferrite and Widmanstätten ferrite. There was no WM solidification cracking evident in the center of the plate (i.e. at the center of the weld length).

3.4. Weld metal solidification cracking

Fig. 4(a-c) shows macrographs of the cross-section (taken within 30 mm from the weld-end) of the 8 , 9.5 and 11 mm welds. Weld centerline cracking is evident in each of these welds. SEM fractography (Fig. 5(a-c)) confirmed that these crack defects are solidification cracks due to the smooth dendritic appearance of the fracture surface. There were no cases of solidification cracking evident in the 5 mm welds.

Plots of the number of welds with solidification cracking (% of total plates welded) and solidification cracking length (% of total weld length) versus parent plate thickness are shown in Fig. 6. Based on the available data, Fig. 6(a) shows that as plate thickness increases, then the likelihood of solidification cracking increases. Fig. 6(b) shows that there is no direct linear relationship between plate thickness and the extent of solidification cracking. The crack lengths were measured from x-ray radiographs, which was also the method used to detect the plates with solidification cracks.

The location of the solidification cracking with respect to the weld microstructure in the 8, 9.5 and 11 mm welds is shown in Fig. 7. The solidification cracking in the 8 mm weld appears to have propagated predominantly along the grain boundary ferrite (Fig. 7 (a-b)). Similarly, the propagation of solidification cracks along grain boundary ferrite is also evident in the 9.5 and 11 mm welds (Figure 7(c-f)). Additionally, there is evidence of fine-scale solidification cracks and some discontinuity in the cracking (Fig. 7 (a-c)).

4. Discussion

Weld metal solidification cracking in the current study was unexpected. Firstly, there are no reported cases in the literature of solidification cracking in PT-GMAW welds. Also, solidification cracking in conventional single-wire GMAW of low alloyed steels is not widely reported. However, Shankar and Devletian [17] do state that the role of C, Ni, S and P is more significant in conventional GMAW than for SAW. Secondly, the outcome of a preliminary analysis on the chemical compositions of the parent steels (Table 1) and the corresponding WM compositions (Table 5) indicated a very low susceptibility to the onset of solidification cracking.

A low solidification crack index, U_{SC}, and a high Mn:S ratio were calculated from the WM compositions in Table 5. The solidification cracking index, U_{SC}, of all weld metals was well below 25 (Table 6), thus indicating a low susceptibility to solidification cracking. Even though these types of equations have been derived from SAW trans-varestraint tests [18], they are commonly used as a point of reference for other arc welding processes. Additionally, the ratio of manganese to sulfur in the four welds (5, 8, 9.5 and 11 mm welds) was between 89 and 140 (Table 6). Adequate levels of Mn are required to tie up sulfur in order to prevent it from segregating to grain boundaries and forming low melting temperature films. For the carbon levels measured in the four weld types (≤0.1 wt %), the calculated Mn:S ratios are overwhelmingly high and, hence, indicate that solidification cracking is not expected to occur [19]. Jones [20] reports that in low alloy steel welds an Mn:S ratio above 50 significantly reduces solidification cracking tendency, and Lancaster [19] states that an Mn:S ratio greater than 10 is required to avoid solidification cracking. However, Ohshita et al. [11] have reported cases of solidification cracking in very low carbon steel welds (≤ 0.1 wt%) using shielded metal arc welding and GMAW.

Despite all of the above, radiographic inspection revealed solidification cracks at the weld-ends within ~30 mm from the run-off tab in many of the test plates. Thus, it can be assumed that the critical levels for inclusion and alloying elements leading to solidification cracking are different for single-bead PT-GMAW than that determined for SAW by transvariant or trans-varestraint tests. These simulated solidification cracking tests may be severe with respect to the loading conditions the weld bead is subjected to during solidification, but weld bead shape is not accurately represented in these types of tests. Hoshino et al. [18] lend support to this view in their assessment of the susceptibility of steel welds to solidification cracking in narrow gap welding, and they subsequently developed an alternative solidification cracking test specific to their situation. It should be noted that in the current work, the length of the solidification cracks was minor (<3% of the total welded length). Even so, crack defects will generally result in a non-compliant weld with all the relevant regulatory standards in naval shipbuilding [21].

The extent of solidification cracking identified in each weld (i.e. 5, 8, 9.5 and 11 mm welds) is quantified in the plots in Fig. 6. Even though these plots are based on limited data, it is evident that as plate thickness is increased the percentage of plates with WM solidification cracking also increased (Fig. 6 (a)), and that crack length is less dependent on plate thickness (Fig. 6(b)). There is no systematic change in WM composition (Table 5) or the solidification cracking index (Table 6) with increasing plate thickness to

support the increase in the number of plates with WM solidification cracking (Fig. 6(a)). Similarly, at the resolution of optical microscopy, there is no significant difference in the WM microstructure (Fig. 3) at the different plate thicknesses to offer an explanation for the increase in the number of plates with solidification cracking as plate thickness is increased. Consequently, the increased cracking that is observed as plate thickness increases is mainly attributed to an increase in the depth-width ratio (Fig. 2). The adverse effect of unfavorable weld bead geometries on the onset of solidification cracking is well known and widely accepted [22]. A decrease in the width of the molten weld pool, which can be related to the depth:width ratio in single bead welds, is shown to have increased susceptibility in solidification cracking [23]. Welded plates with higher thickness are also associated with increased restraint and increased tensile residual stresses, both of which could also increase susceptibility to solidification cracking.

The microstructure of the weld bead in the center of the welded plate is similar to the microstructure at the weld-end (where the solidification cracks are located). This suggests that there are no microstructural features (at the resolution of optical microscopy) peculiar to the weld-end responsible for the onset of solidification cracking (compare microstructures in Fig. 3 to corresponding microstructures in Fig. 7). Makarov et al. [23] attribute solidification cracking at the weld-ends to the strain rate in the temperature range of brittleness (TRB) zone, which is the greatest at the weld ends compared with the weld-start and weld-center. Makarov et al. [23] specifically address the issue of solidification cracking at the weld-ends of 10 mm shipping steel plate. The cracking described by them in single-sided multi-wire SAW is remarkably similar to that observed in the current work with PT-GMAW and that encountered by naval shipbuilders in Australia with SAW. In a less detailed study, Hoshino et al. [18] attribute solidification cracking in narrow gap welds to the speed of displacement of the parent steel (proportional to strain rate in the TRB).

The TRB zone is the area immediately trailing the fully molten weld pool, and its size is dependent on factors such as weld process type, heat input and plate thickness. This strain rate in the TRB zone (B_{TRB}), which must exceed a threshold or critical strain rate for solidification cracking to occur, is directly proportional to the rate of transverse displacement in the plate ahead of the molten weld pool (V_t), and inversely proportional to the cooling rate of the TRB zone (W_0) (see Eq. 1). Equation 2 shows that B_{TRB} is also proportional to the length of the TRB zone (l_{TRB}) and inversely proportional to welding travel

speed (V_w), temperature range of the TRB zone (TRB) and the width of the molten weld pool (h_p) [23]. In contrast, Morgan-Warren and Jordan [24] report that an increase in weld travel speed increases the length of the crack-susceptible zone (l_{TRB}) but decreases the transverse crack-promoting forces.

$$B_{TRB} = V_t / W_0 \qquad \text{(Equation 1)}$$

$$B_{TRB} \approx V_t \times l_{TRB} / \left(V_w \times TRB \times h_p \right) \qquad \text{(Equation 2)}$$

The work of Makarov et al. [23] is considered relevant to the solidification cracking discovered in the current program, despite some of the obvious differences between the two studies. Firstly, the work carried out by them was based on SAW. However, the location of the cracking, the role of the run-off tabs, the end-user application and the plate thickness justifies drawing on this publication for reference. Secondly, the work of Makarov et al. [23] was based on plates secured on one side, but extensive modeling work carried out by them showed that securing plates on both sides by clamping would only have a minor secondary effect on the rate of transverse displacement. In the current study, all plate halves were clamped prior to welding.

There are particular characteristics of the single-bead PT-GMAW process that contribute to weld-end solidification cracking in the welding of the naval steels in the current work. These include (i) weld travel speeds (shown in Table 4) above the threshold for solidification cracking [11], (ii) a long trailing weld pool compared with conventional single-wire GMAW that increases the length of the susceptible region (TRB zone), (iii) the ability to use a single-bead weld, which unlike multiple-bead GMAW does not allow for the back-gouging of often problematic first (i.e. root) runs [11], and (iv) higher deposition rates (and higher arc energy heat inputs) compared with conventional single-wire GMAW resulting in a slower cooling rate and increasing the likelihood of solidification cracking [23].

Solidification cracks located at the weld-ends and formed during the single-bead PT-GMAW of naval hull steels should be avoidable. Makarov et al. [23] explains that the run-off tab system used will influence the rate of transverse displacement in the parent steels, and ultimately the likelihood of solidification cracking. In the current work, run-off tabs (80 mm x 100 mm plates) without grooves and attached to the main test

plate by tacking on either side of the weld preparation were used. Makarov et al. [23] reported that a 150 mm long groove in the run-off tab for the oncoming weld to fill will significantly reduce the rate of transverse displacement, and hence reduce the likelihood of solidification cracking. Alternatively, targeted heating at the weld-ends prior to welding will reduce the likelihood of solidification cracking by 7 times [23]. However, the targeted heating approach is undesirable in naval shipbuilding because it is costly and time consuming, and if incorrectly applied could adversely impact the integrity of the hull. A successful technique currently being used in some Australian naval shipbuilding yards for the PT-GMAW of 12 mm thick DH36 steel plate is to adopt a single-sided multiple-run weld with a temporary backing strip [6]. This technique allows; (i) the manipulation of the weld process parameters to obtain a desirable weld-bead shape that is less prone to solidification cracking, and (ii) improves the impact toughness of the WM due to the tempering effect from ensuing weld beads. However, there is an adverse impact of this technique on shipyard productivity compared with single-sided single-bead welding.

The solidification cracks found in the 11 mm weld were less severe than those found in the other welds. Cracks in the 11 mm welds were not as long and deep compared with those in the 8 mm and 9.5 mm welds (compare Fig. 4(c) with Fig. 4(a-b)). This was also confirmed in the radiographs of the 11 mm weld by their relatively short lengths and lighter appearance. The small size of the solidification cracks in the 11 mm weld, despite it having the greatest weld bead depth-width ratio, is attributed to a significantly lower level of Ni in the WM. The 11 mm weld measured at least 5 times less Ni than 8 mm weld and 10 times less Ni than 9.5 mm weld (compare Ni contents in Table 5). Nickel is reported to increase solidification-cracking tendency as it widens the TRB zone, increase the solidification temperature range, increase the liquidus temperature, and acts in combination with sulfur to form low melting point nickel sulfides [25]. In further support on the role of Ni in weld metal solidification cracking, Masumoto and Imai [26] report on the segregation of Ni at dendritic boundaries in steel welds. Other elements such as Ti, Al, Cu, S and Ca were detected by EDS in some locations of the fracture surfaces on both the 8 mm and 11 mm HSLA65 welds, but it was not possible to establish the effect that they had on either the likelihood or extent of solidification cracking.

Optical microscopy, SEM and EDS were used to characterize the cracks located near the end of the welds, and to gain insight into the potential mechanisms of crack initiation and the propagation path. The smooth dendritic appearance of the fracture surfaces examined (Fig. 5(a-c)), confirmed that the cracks in the welded test plates were solidification cracks. Semi-quantitative EDS analysis showed that sulfur

played an integral role in the solidification cracking observed. Approximately twice the amount of sulfur was detected on the fracture surface of the solidification cracks compared with sulfur levels distant from the cracks (also measured by EDS for consistency).

Fig. 7 shows optical micrographs of WM solidification cracking and the surrounding microstructure in the 8, 9.5 and 11 mm welds. The solidification cracks in these welds are mainly situated along the grain boundary ferrite (Fig. 7). The carbon levels in the 8, 9.5 and 11 mm welds are respectively, 0.08 wt%, 0.05 wt%, and 0.07 wt% (Table 5). Ohshita et al. [11] report that at these very low levels of carbon, solidification cracking will occur along the delta ferrite grain boundaries during delta-phase solidification. However, this aspect has not been investigated in the current study. Additionally, the presence of fine/small solidification cracks (labeled in Fig. 7(a and c)) that appear detached from the main crack could be connected to the main crack on planes outside of the cross-section shown in these macrographs.

5. Conclusions

The following conclusions are drawn from the current work.

1. Single-bead welds produced by PT-GMAW can be susceptible to WM solidification cracking near the weld-end (within 30 mm from the run-off tab). Characteristic features of the single-bead PT-GMAW process which contribute to this type of cracking include high weld travel speeds, a long trailing weld pool, high deposition rates and slow cooling rates compared with welding procedures that would be used for conventional single-wire GMAW.
2. The incidence of WM solidification cracking was found to increase with increasing plate thickness. This was attributed to an increase in the weld bead depth:width ratio and joint restraint with increasing plate thickness, and critical levels of impurity and alloying elements in the weld metal.
3. The sizes of solidification cracks in the 11 mm weld were smaller than the cracks in the 8 and 9.5 mm welds. Weld metal with significantly less Ni was attributed to limiting the size of the solidification cracks.
4. The levels of impurity elements (S and P) measured in the weld metal were significantly lower than that reported to increase the risk of solidification cracking in solidification cracking in submerged arc welds. Similarly, the Mn:S ratios calculated for each of the weld metals were substantially greater than that reported to increase the risk of solidification cracking in the literature that was reviewed.

Acknowledgements

The authors would like to acknowledge the Defence Materials Technology Centre (DMTC) for their ongoing support. We would also like to thank Dr Len Davidson, Dr Stan Lynch and Dr Stuart Cannon from DSTO for their support of this work and review of this paper. The authors would also like to acknowledge the support of Dr Allison Nolting, Mr Cameron Munro and Alexandra McLeod from DRDC Atlantic, Mr Johnnie DeLoach from NSWC–Carderock Division, and Prof. John Norrish from University of Wollongong. We also gratefully acknowledge the efforts of Mr Paul Calleja, Mr Joseph Dominguez and Mr Frank Griffo from DSTO for their assistance with welding, welding preparation, post-weld sectioning, and SEM EDS analysis.

References

1. Yudobidroto, B. Y. B., Hermans, M. J. M., Richardson, I. M., 2006. The influence of pulse synchronisation on the process stability during tandem wire arc welding. IIW Doc. No. XII-1910-06, International Institute of Welding.
2. Sterjovski, Z., Donato, J., Li, H., 2011. The effect of travel speed and CTWD on the bead profile and microstructure of tandem GMA steel welds. *Australasian Welding Journal*, 1st Quarter, pp 40-46.
3. Sterjovski, Z., Donato, J., Munro, C., Lane, N., Luzin, V., Larkin, N., 2011, An Evaluation of Pulsed Tandem GMAW of HSLA65 steel for Naval Shipbuilding. 6th Asian Pacific IIW International Congress and 56th WTIA Annual Conference, Cairns, Australia, 25-27 September
4. Sampath, K., 2006. An understanding of HSLA-65 Plate Steels. *Journal of Materials Engineering and Performance*, 15(1), 32-40.
5. Barsoum, R. G. S., 2005. United States Patent – Hybrid Ship hull, US 6941888B2.
6. Lang, D., 2012. Weld Procedure Qualification PQR-7139-Tandem GMAW, single-side welded single vee butt weld-12 mm ASTM A322 DH36. Forgacs Engineering Pty Ltd.
7. Sterjovski, Z., Donato, J., Munro, C., Lane, N., Luzin, V., Larkin, N., 2011. Application of pulsed tandem gas metal arc welding for fabrication of high strength steel panels in naval surface vessels. Australasian Welding Journal, 4, 37-48.
8. Larkin, N., Pan, Z., van Duin, S., Lane, N., Li, H., 2010. Feasibility testing of T-GMAW for Low Distortion Butt Welds. DMTC Report.
9. Sutton, B. J., 2013. Solidification behavior and hot cracking of high manganese steel weld metals, Thesis, The Ohio State University.
10. Kannengiesser, T., Rethmeier, M., Portella, P. D., Ewert, U., Redmer, B., 2011. Assessment of hot cracking behaviour in welds. *Int. J. Mat. Res.*, 102(8), 1001.
11. Ohshita S., Yurioka N., Mori N., Kimura T., 1983. Prevention of solidification cracking in very low carbon steel welds. *Welding Journal*, 62(5), 129.
12. Machado, I. G., 1984. Weldability aspects of high yield strength Q and T steels. PhD Thesis, Cranfield Institute of Technology.
13. ASTM International, 2008. A131M-08.
14. Canadian Standards Association, 2004. G40.20, General Requirements for Rolled or Welded Structural Quality Steels, Mississauga ON, 2004.
15. ASTM International, 2006. A945/A945M-06.
16. Standards Australia, 2006. AS2177-2006.
17. Shankar, V., Devletian, J. H., 2005. Solidification cracking in low alloy steel welds. *Science and Technology of Welding and Joining*, 10(2), 236.
18. Hoshino, K., Yamashita, R., Shinoda, T., Ono H., 1988. Solidification Cracking in Narrow Gap Welded Joints, Proc. 7th International Conference on Offshore Mechanics and Arctic Engineering, Houston, Texas, February 7(12), 45.
19. Lancaster, J. F., *Metallurgy of Welding*, 6th Ed., Abington Publishing, Cambridge England, 1999.

20. Jones, P. W., 1959. An investigation of hot cracking in low-alloy steel welds, *British Welding Journal*, 6 (6), 282-290.
21. McLeod, A., Bayley C., 2012. Microstructural investigation of PT-GMAW welding defects. Letter Report, DRDC Atlantic/DLP/3771-7-2.1203776, DRDC Atlantic.
22. Messler, R. W., Jr, 2004. *Principles of Welding- Processes, Physics, Chemistry and Metallurgy*. Wyley-VCH, Weinhein.
23. Makarov, E., Herold, H., Schhtraitenberg, M., Pshennikov, A., 2000. Preventing hot cracking in end sections of long welds in one-sided, multi-arc, submerged-arc welding. *Welding International*, 14(4), 305-309.
24. Morgan-Warren, E. J., Jordan, M. F., 1976. Effect of travel speed on solidification cracking in autogenous tungsten inert gas arc welding of low-alloy steel sheet. *Metals Technology*, 1, 29-39.
25. Matsuda, F., Savage, W. F., 1969. Effect of individual alloying element on hot-cracking of two low alloy steels, Technical Report, Osaka University, 19(867/907), 467-491.
26. Masumoto, I. and Imai, K., 1970. A metallurgical aspect of hot cracking and toughness of weld metal, *Trans. Jap. Weld Res, Inst.*, 1(1), 104-111.

*Figure 1
Click here to download high resolution image

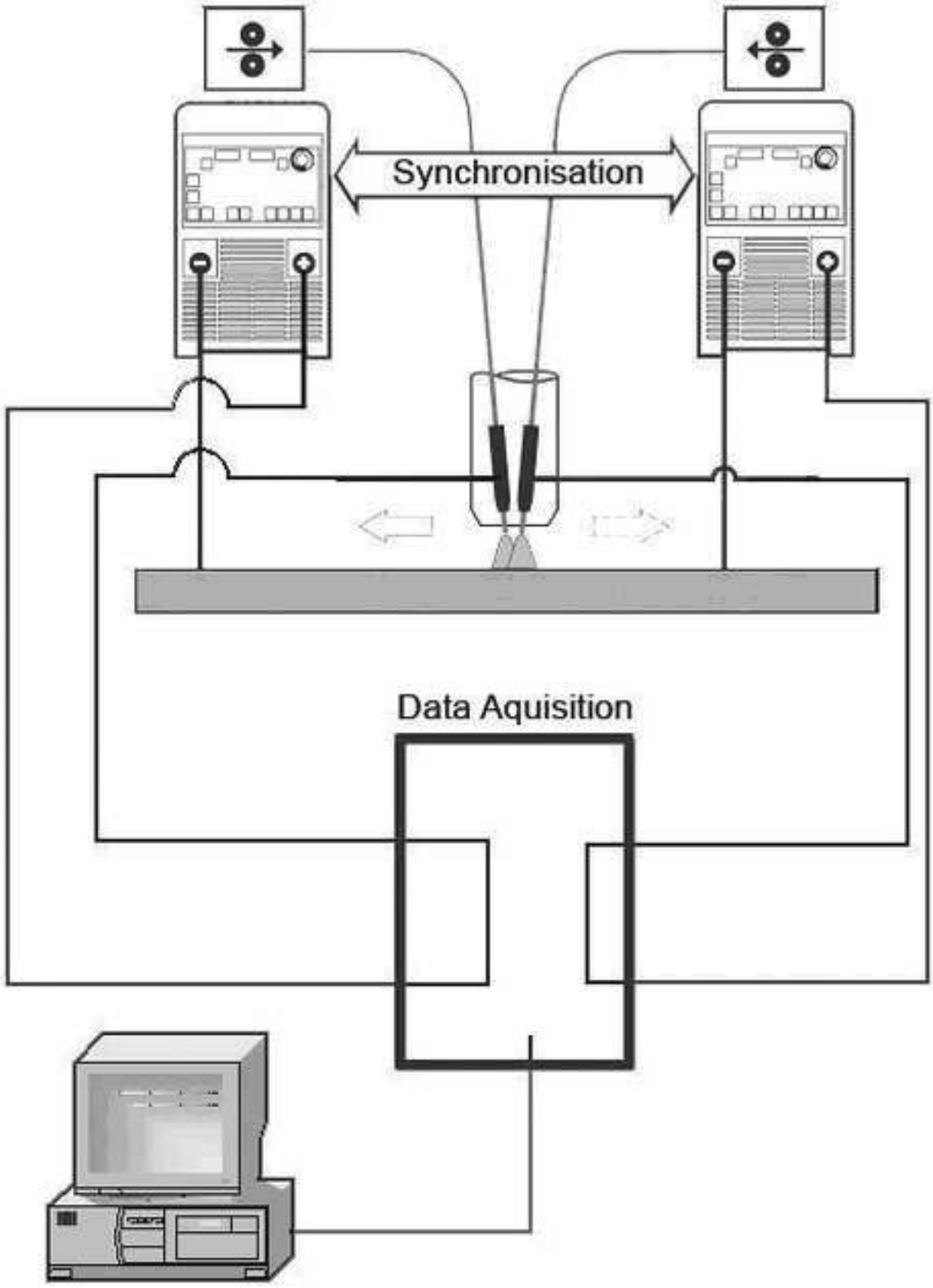

*Figure 2
Click here to download high resolution image

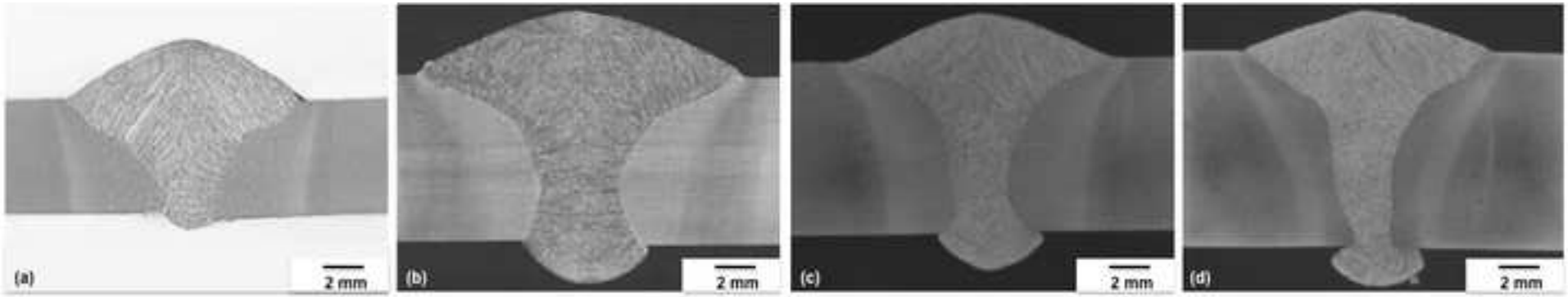

*Figure 3
Click here to download high resolution image

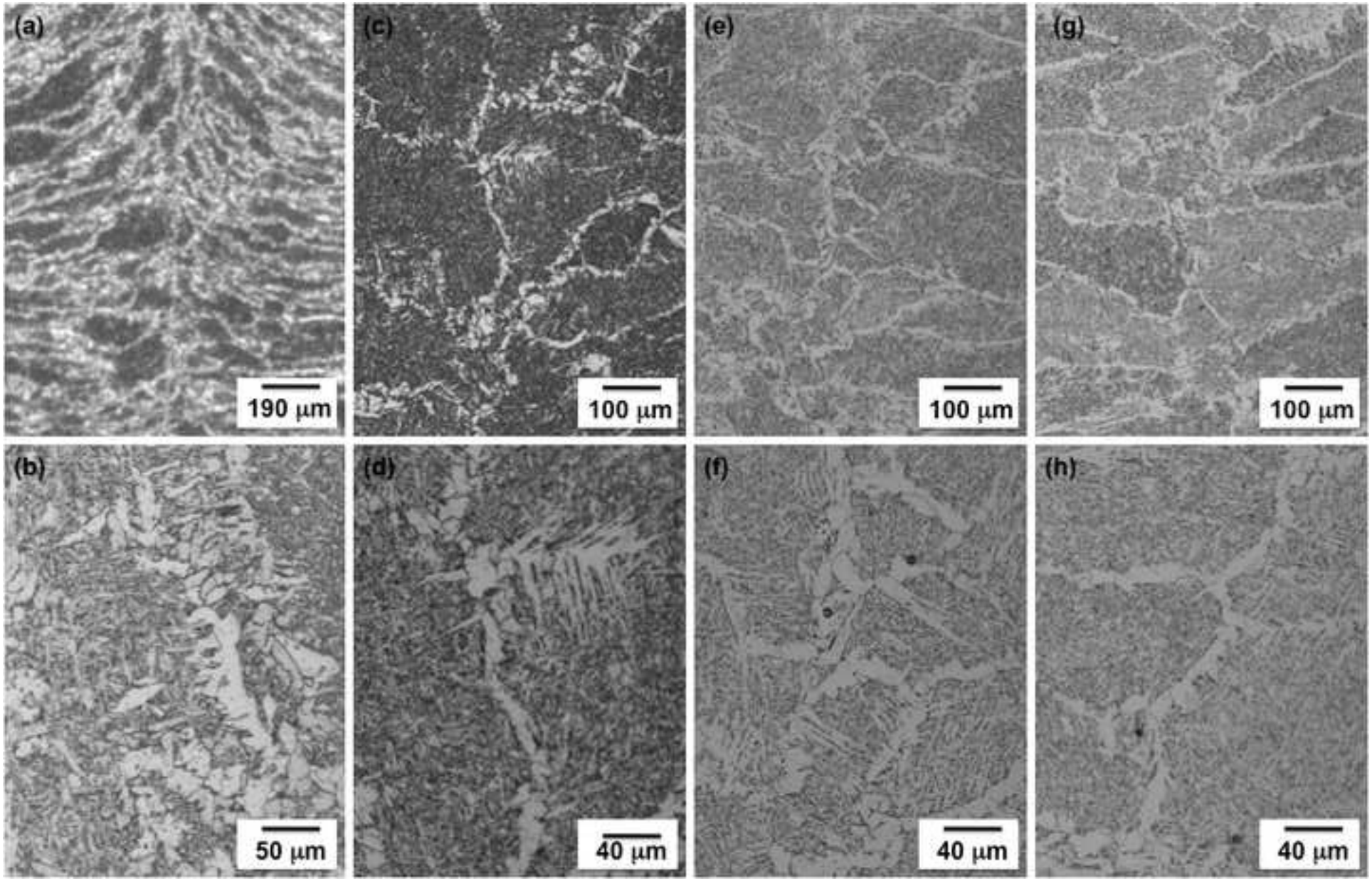

*Figure 4
Click here to download high resolution image

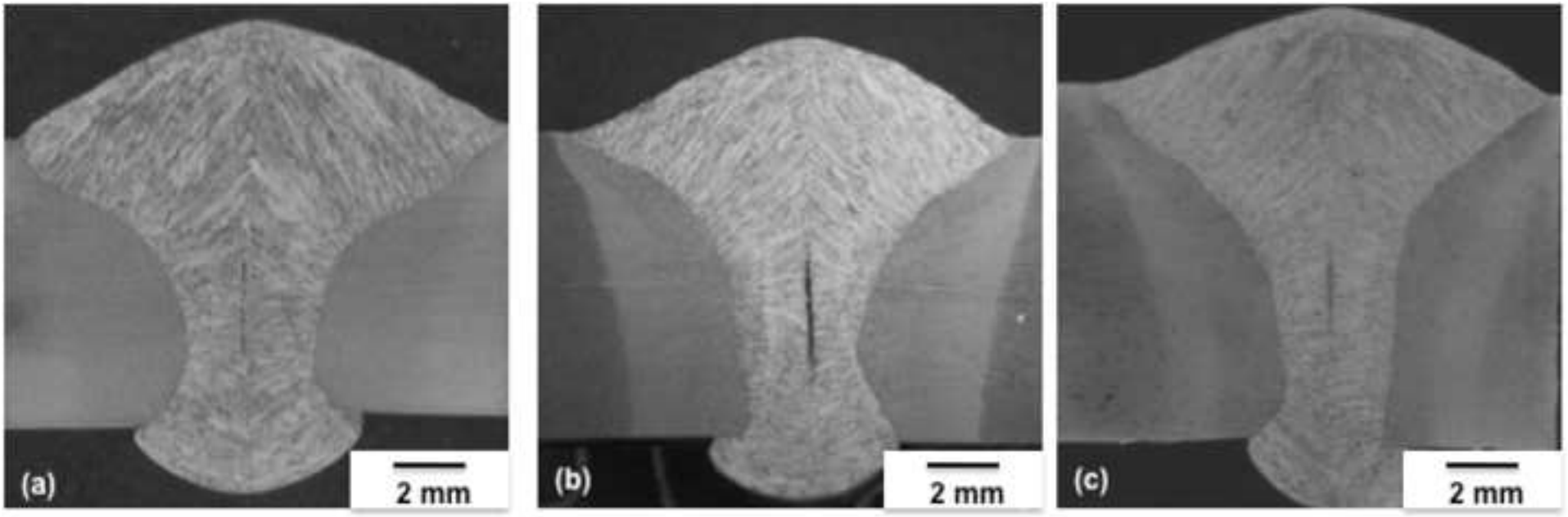

*Figure 5
Click here to download high resolution image

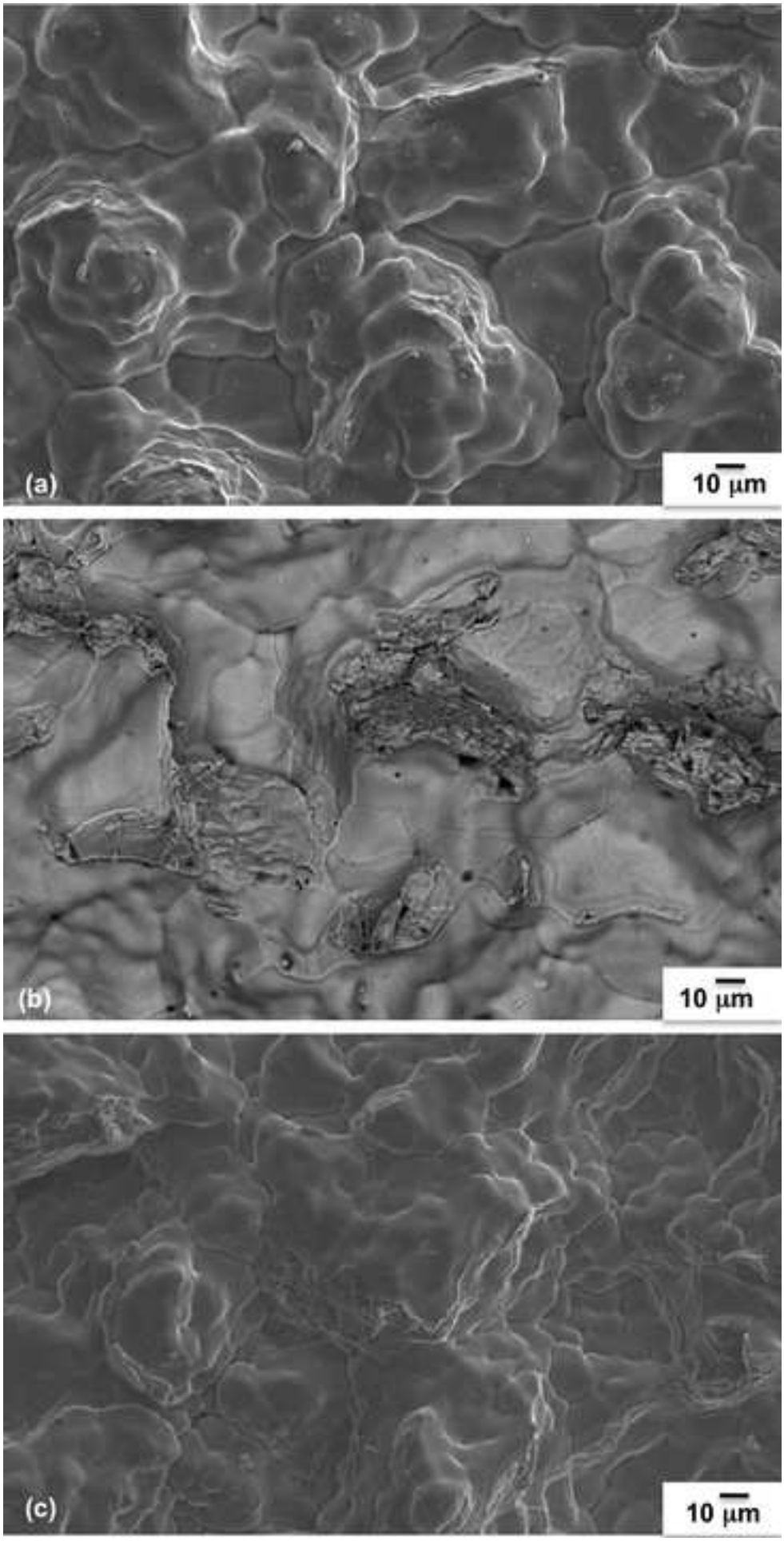

*Figure 6
Click here to download high resolution image

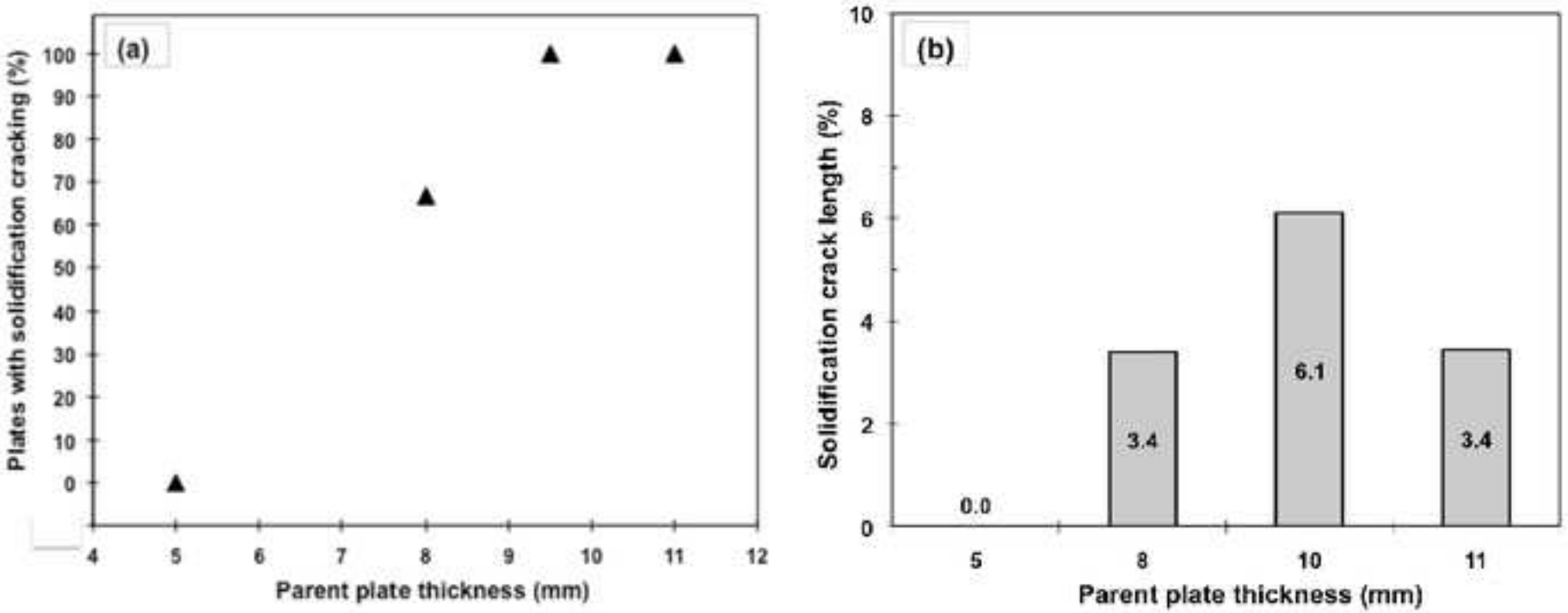

*Figure 7
Click here to download high resolution image

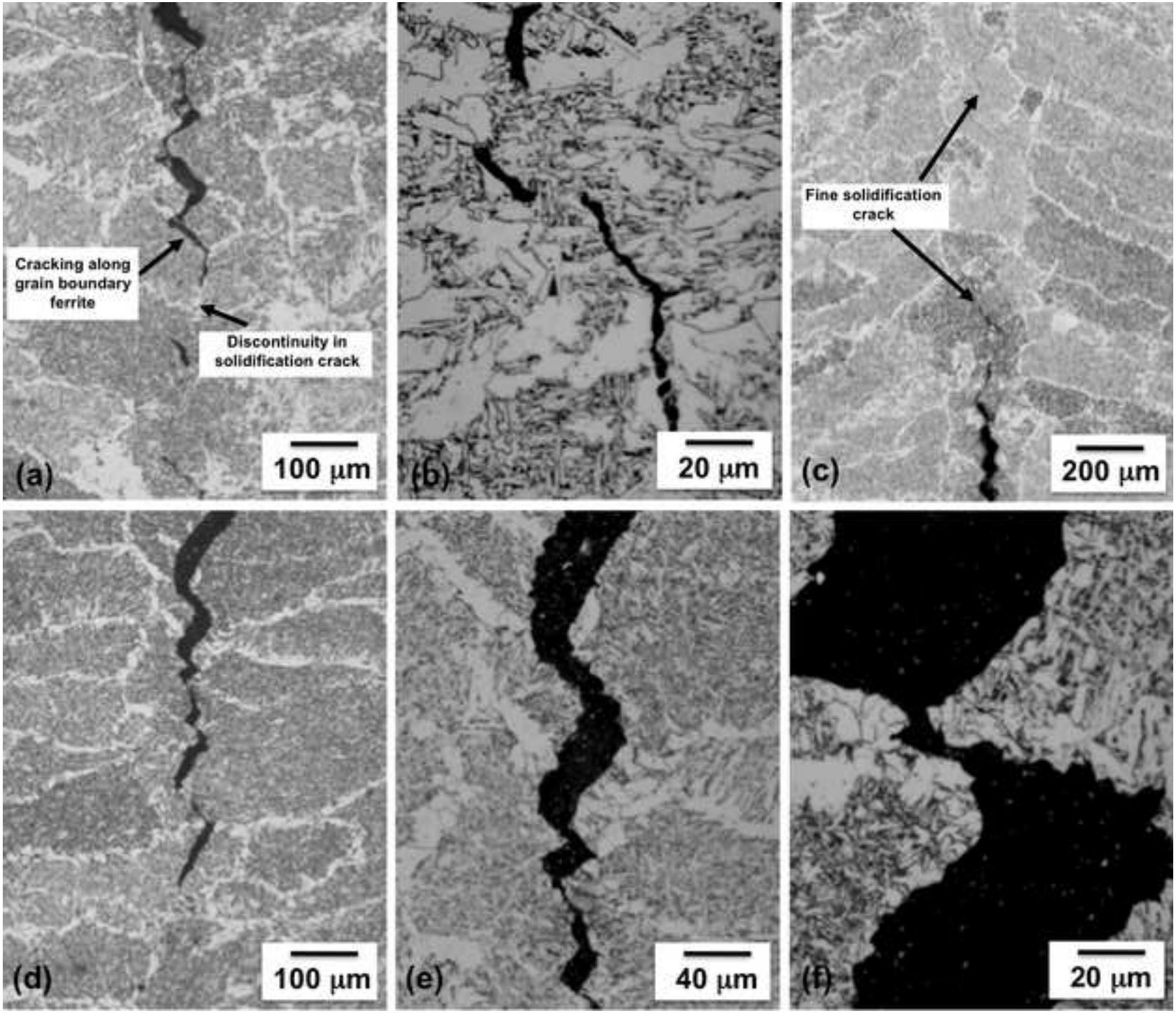

*Figure Caption List

Fig. 1. Schematic layout of the PT-GMAW welding equipment used for the experimental program.

Fig. 2. Typical macrographs of the welded cross-sections (from the weld centre) of the: (a) 5 mm weld; (b) 8 mm weld; (c) 9.5 mm weld; and (d) 11 mm weld, showing an increase in the weld bead depth: width ratio as thickness increases. Etched in 2% Nital.

Fig. 3. Optical micrograph of the WM microstructure (from the weld centre) of (a-b) 5 mm weld, (c-d) 8 mm weld, (e-f) 9.5 mm weld, and (g-h) 11 mm weld showing no significant differences in microstructure for the four weld types. Etched in 2% Nital.

Fig. 4. Macrographs showing the welded cross-sections (~30 mm from the weld-end) of the: (a) 8 mm weld; (b) 9.5 mm weld; and (c) 11 mm weld, revealing WM solidification cracking. Etched in 2% Nital.

Fig. 5. Typical SEM images of the fracture surface confirming solidification cracking in the: (a) 8 mm weld (SE); (b) 9.5 mm weld (BSE); and (c) 11 mm weld (SE).

Fig. 6. Plot of (a) number of welded plates with solidification cracking (%) versus plate thickness showing that the incidences of solidification cracking increases with increasing plate thickness, and (b) solidification crack length (%) versus plate thickness showing that the extent of cracking is not linear with plate thickness.

Fig. 7. Optical micrographs showing the WM solidification crack and surrounding microstructure for (a-b) 8 mm weld, (c) 9.5 mm weld, and (d-f) 11 mm weld. Etched in 2% Nital.

Table 1

Click here to download high resolution image

5 mm DH36	**C**	**Mn**	**Si**	**S**	**P**	**Ni**	**Cr**	**Mo**
	0.14	1.39	0.34	0.015	0.012	0.017	0.01	0.01
	Al	**B**	**N**	**O**	**Cu**	**V**	**Nb**	**Ti**
	0.039	<0.0005	0.002	N/A	0.019	0.01	0.001	0.015
8 mm H SLA65	**C**	**Mn**	**Si**	**S**	**P**	**Ni**	**Cr**	**Mo**
	0.08	1.39	0.22	0.007	0.011	0.38	0.14	0.09
	Al	**B**	**N**	**O**	**Cu**	**V**	**Nb**	**Ti**
	0.009	<0.0005	0.006	<0.01	0.24	0.063	0.020	0.010
9.5 mm CSA 350WT	**C**	**Mn**	**Si**	**S**	**P**	**Ni**	**Cr**	**Mo**
	0.05	1.29	0.22	0.006	0.011	0.10	0.17	0.02
	Al	**B**	**N**	**O**	**Cu**	**V**	**Nb**	**Ti**
	0.027	<0.0005	0.006	<0.005	0.23	0.05	0.04	<0.1
11 mm H SLA65	**C**	**Mn**	**Si**	**S**	**P**	**Ni**	**Cr**	**Mo**
	0.07	1.49	0.28	0.007	0.011	0.01	0.03	0.02
	Al	**B**	**N**	**O**	**Cu**	**V**	**Nb**	**Ti**
	0.018	<0.0005	0.005	<0.01	0.01	0.072	0.03	0.015

Table 2

Click here to download high resolution image

	C	Mn	Si	S	P
ER70S-6	0.07	1.55	0.88	0.012	00.015

Table 3
Click here to download high resolution image

Weld ID	Weld Wire	Parent Steel	Weld Lengths (mm) (and no. of plates)	Total Weld Length (mm)
5 mm weld	ER70S-6	DH36	700 (4)	2800 mm
8 mm weld	ER70S-6	HSLA65	700 (1), 350 (8)	3500 mm
9.5 mm weld	ER70S-6	CSA 350WT	450 (4)	1800 mm
11 mm weld	ER70S-6	HSLA65	450 (2), 350 (1)	1250 mm

Table 4

Click here to download high resolution image

	5 mm weld	8 mm weld	9.5 mm weld	11 mm weld
Weld Preparation	square butt	square butt	square butt	square butt
Root Gap	0 mm	1.2 mm	1.6 mm	1.8 mm
Mode	Pulse(L [a] & T [b])	Pulse(L & T)	Pulse(L & T)	Pulse(L & T)
Preheat (°C)	20	20	20	20
Gas Flow rate (l/min)	15(L & T)	15(L & T)	15(L & T)	15(L & T)
Welding Position	Downhand	Downhand	Downhand	Downhand
Torch Angle (°)	90(L) / 80 (T)	90(L) / 80 (T)	90(L) / 80 (T)	90(L) / 80 (T)
Polarity	DC+ (L & T)	DC+ (L & T)	DC+ (L & T)	DC+ (L & T)
Wire Feed Speed (m/min)	14(L) / 14(T)	16(L) / 12(T)	16(L) / 12(T)	16(L) / 12(T)
Deposition Rate (kg/hour)	14.91	14.91	14.91	14.91
CTWD [c] (mm)	20	25	25	25
Average Current (A)	325(L) / 308(T)	345(L) / 270(T)	345(L) / 270(T)	345(L) / 270(T)
Average Voltage (V)	31.0(L) / 31.0(T)	32.8(L) / 30.5(T)	32.8(L) / 30.5(T)	32.8(L) / 30.5(T)
Travel Speed (mm/min)	1200	750	750	720
Heat Input (kJ/mm)	0.50 (L) / 0.48 (T)	0.90 (L) / 0.66 (T)	0.90 (L) / 0.66 (T)	0.94 (L) / 0.69 (T)

Table 5

Click here to download high resolution image

5 mm Weld	C	Mn	Si	S	P	Ni	Cr	Mo
	0.10	1.16	0.44	0.013	0.016	0.02	0.04	0.01
	Al	B	N	O	Cu	V	Nb	Ti
	0.019	<0.0005	0.006	0.029	0.08	0.01	<0.01	0.01
8 mm Weld	C	Mn	Si	S	P	Ni	Cr	Mo
	0.08	1.12	0.43	0.008	0.010	0.20	0.09	0.05
	Al	B	N	O	Cu	V	Nb	Ti
	0.008	N/A	N/A	0.034	0.21	0.008	0.013	0.005
9.5 mm Weld	C	Mn	Si	S	P	Ni	Cr	Mo
	0.06	1.11	0.41	0.008	0.009	0.10	0.10	0.02
	Al	B	N	O	Cu	V	Nb	Ti
	0.007	<0.0005	0.007	0.044	0.20	0.03	0.02	<0.01
11 mm Weld	C	Mn	Si	S	P	Ni	Cr	Mo
	0.07	1.22	0.42	0.010	0.010	0.02	0.03	0.02
	Al	B	N	O	Cu	V	Nb	Ti
	0.019	<.0005	0.006	0.029	0.09	0.04	0.02	0.01

Table 6

Click here to download high resolution image

Weld ID	Solidification Cracking Index, U_{SC} [a]	Mn: S Ratio	Solidification Cracking
5 mm weld	14.1	89	No
8 mm weld	8.7	140	Yes
9.5 mm weld	4.6	139	Yes
11 mm weld	6.5	122	Yes

[a] USC = 230C+190S+75P+45Nb-12.3Si-5.4Mn-1

*Table Caption List
Click here to download Table: Sterjovski_WJ_TableCaptions.doc

Table 1
Actual chemical composition (wt %) of the hull steels investigated. Balance is Fe.

Table 2
Nominal chemical composition (wt %) of the ER70S-6 welding wire. Balance is Fe.

Table 3
List of butt-welds completed and corresponding weld lengths.

Table 4
Weld preparation details and key process parameters for the 5 mm DH36, 8 mm HSLA65, 9.5 mm CSA 350WT, and 11 mm HSLA65 welds (ER70S-6 wire).

Table 5
Actual weld metal chemical composition (wt %) using the ER70S-6 wire. Balance is Fe.

Table 6
Solidification cracking index and Mn:S ratio for all the welds. For butt-welds an U_{SC} value over 25 indicates susceptibility to cracking [19].